Journal of
Materials Chemistry A

Accepted Manuscript

This is an *Accepted Manuscript*, which has been through the RSC Publishing peer review process and has been accepted for publication.

Accepted Manuscripts are published online shortly after acceptance, which is prior to technical editing, formatting and proof reading. This free service from RSC Publishing allows authors to make their results available to the community, in citable form, before publication of the edited article. This *Accepted Manuscript* will be replaced by the edited and formatted *Advance Article* as soon as this is available.

To cite this manuscript please use its permanent Digital Object Identifier (DOI®), which is identical for all formats of publication.

More information about *Accepted Manuscripts* can be found in the **Information for Authors**.

Please note that technical editing may introduce minor changes to the text and/or graphics contained in the manuscript submitted by the author(s) which may alter content, and that the standard **Terms & Conditions** and the **ethical guidelines** that apply to the journal are still applicable. In no event shall the RSC be held responsible for any errors or omissions in these *Accepted Manuscript* manuscripts or any consequences arising from the use of any information contained in them.

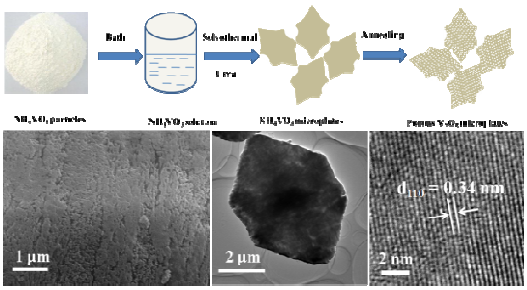

Three-dimensional porous V_2O_5 quasi-hexagonal hierarchical microplates with tunable porosity were fabricated by a one-step top-down strategy.

Cite this: DOI: 10.1039/c0xx00000x

www.rsc.org/xxxxxx

Communication

Top-Down Fabrication of Three-Dimensional Porous V_2O_5 Hierarchical Microplates with Tunable Porosity for Improved Lithium Batteries†

Qinyou An,‡ Pengfei Zhang,‡ Qiulong Wei, Liang He, Fangyu Xiong, Jinzhi Sheng, Qinqin Wang and Liqiang Mai*

Received (in XXX, XXX) XthXXXXXXXXX 20XX, Accepted Xth XXXXXXXXX 20XX
DOI: 10.1039/b000000x

3D porous V_2O_5 hierarchical microplates have been fabricated by a one-step top-down strategy, and display excellent rate capability and stable capacity of 110 mAh g^{-1} at 2000 mA g^{-1} after 100 cycles. We have demonstrated the facile approach of a solid-phase conversion is promising for large-scale fabrication of highly porous micro/nano materials.

Introduction

The ever increasing demand in electrochemical devices with advanced energy conversion and storage has stimulated significant interests in lithium battery (LB) research.[1-3] The lithium battery is one of the most promising energy storage systems which is efficient in delivering energy, light in weight and environmentally benign.[4-7] For the application in electric vehicles (EVs) and hybrid electric vehicles (HEVs), the energy density of LBs still need to be improved.[7-9] Increasing the energy density of LBs requires the development of electrode materials with higher capacity.[8-12] Among the potential cathode materials, vanadium pentoxide (V_2O_5) with a layered structure has been extensively investigated due to its low cost, abundance as well as its high theoretical capacity (about 294 mAh g^{-1} with 2 Li insertion/extraction per unit formula).[13-17] Even only one Li insertion/extraction, it also can deliver a comparable capacity compared to the commercialized cathode materials such as $LiCoO_2$ (140 mAh g^{-1}) and $LiMn_2O_4$ (146 mAh g^{-1}).[13,18-20] However, two critical issues for this electrode material are its low rate and limited long-term cycling stability, due to its slow electrochemical kinetics and poor structural stability.[21-23]

In the last decades, many efforts have been focused on the synthesis of micro/nano-structured vanadium oxides to mitigate the slow electrochemical kinetics by acquiring high surface area and short ion/electron diffusion distance.[24] Various micro/nano-structures reported with different performance suggest that the characteristics of V_2O_5, such as the dimensions, morphology, porosity, and texture, are critically important for the electrochemical performance of the electrodes.[25-27] In particular, V_2O_5 nanostructures, such as nanowires, nanorods, nanoribbons, nanosheets and hollow structures can prove to improve the electrochemical kinetics effectively, shorten the diffusion distance for Li^+ ions, and buffer the volume change, maintaining mechanical integrity and chemical stability over many intercalation/deintercalation cycles as compared with non-nanostructured materials.[28-30] However, the electrochemical performance of V_2O_5 nanomaterials, particularly, the cycling stability and rate capability, is still not very satisfactory. As is well-known, porous aggregates of electrode materials show great advantages such as good contact with electrolyte, high specific surface area, improved Li^+ permeation and easier to bind than isolated nanosized particles, which can reduce the polarization and decrease the structure stress during the charge/discharge processes.[31-36] Furthermore, the hierarchical structures can effectively prevent the self-aggregation of electrode materials upon cycling.[36] Thus, constructing the V_2O_5 cathode material with hierarchical porous structure has been considered to be a valid way to improve its electrochemical performance.

Creating an open pore-network within the bulk of the solid is an effective approach to form hierarchical porous cathode materials.[37] In this work, we report a facile top-down preparation of porous nanoarchitectures from large microcrystals. To the best of our knowledge, it may be the first time to synthesize the three-dimensional (3D) porous V_2O_5 quasi-hexagonal hierarchical microplates with tunable porosity. When evaluated as a cathode material for LBs, the porous V_2O_5 microplates manifest significantly improved electrochemical performance in terms of specific capacity, cycling stability and rate capability.

Experimental Section

Materials synthesis

In a typical synthesis, urea (1.5 g) and NH_4VO_3 (0.1 mmol) were dissolved in 10 mL deionized water in turn under vigorous stirring at 80 °C. After stirring for 20 min, 50 mL acetonitrile was added into the above solution, and then the solution was continued to stirring for 1 h. Sequentially, the mixture was transferred into a Teflon-lined stainless steel autoclave with a capacity of 100 mL. After heating at 180 °C for 12 h, the autoclave was naturally cooled to room temperature, and the precipitate was collected by centrifugation and washed three times with ethanol. Finally, 3D porous V_2O_5 hierarchical microplates were obtained by annealing the solvothermally prepared NH_4VO_3 quasi-hexagonal microplates in air at 350 °C for 2 h with a heating rate of 2 °C min^{-1}. A series of experiments

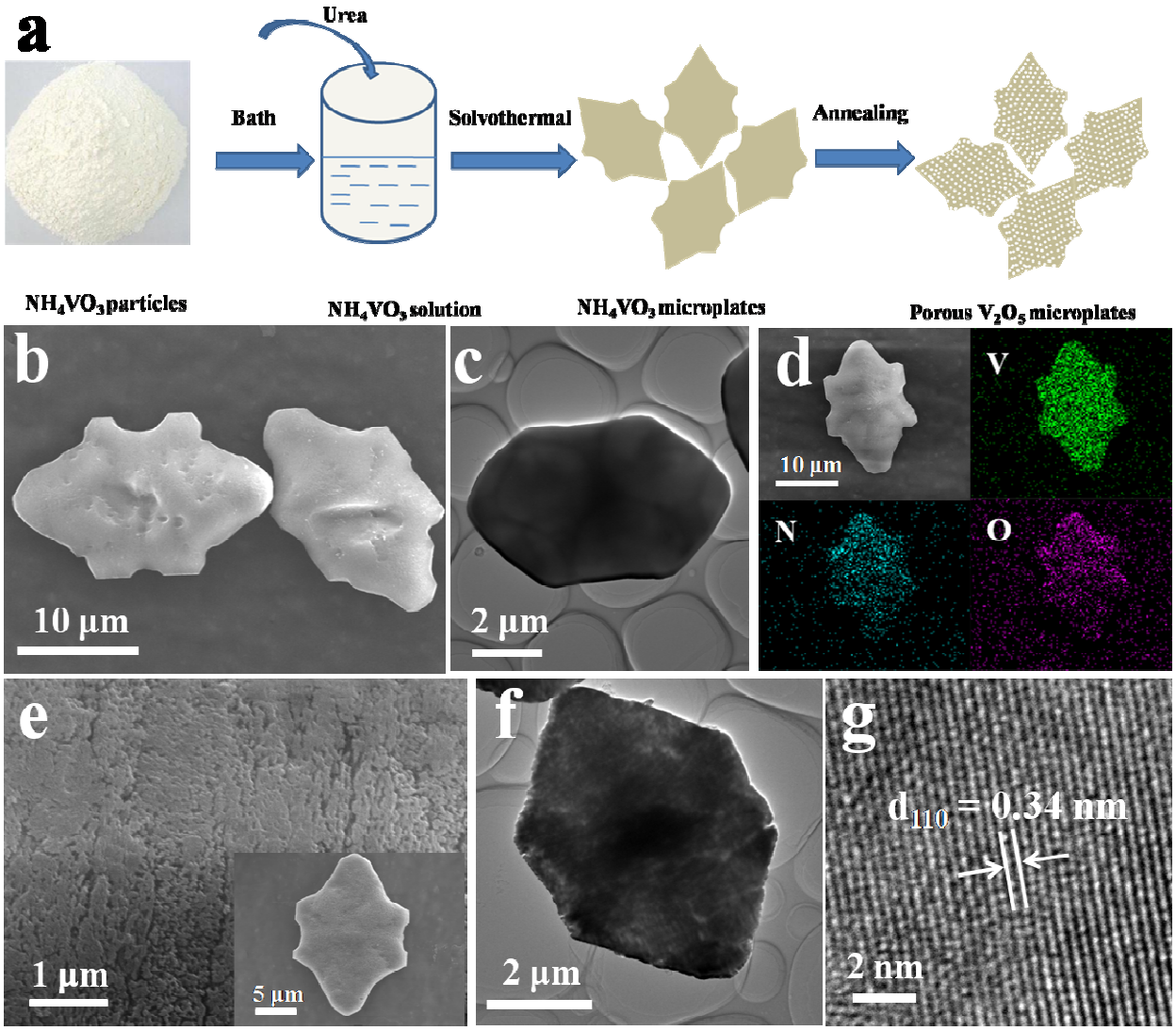

Figure 1. (a) A schematic illustration for the formation of 3D porous V_2O_5 hierarchical microplates through one-step thermal decomposition of NH_4VO_3 microcrystals. FESEM image (b), TEM image (c) and EDS mapping (d) of NH_4VO_3 quasi-hexagonal microplates. FESEM (e), TEM (f) and HRTEM (g) images of the 3D porous V_2O_5 hierarchical microplates annealed at 350 °C.

were also carried out at different solvothermal reaction times and calcination temperatures to investigate the structural evolution process.

Characterization

X-ray diffraction (XRD) measurements were performed to investigate the crystallographic information using a D8 Advance X-ray diffractometer with non-monochromated Cu Kα X-ray source. Field emission scanning electron microscopy (FESEM) images were collected with a JEOL-7100F microscopy at an acceleration voltage of 10 kV. Transmission electron microscopy (TEM) images and high-resolution transmission electron microscopy (HRTEM) images were recorded by using a JEM-2100F STEM/EDS microscope. Brunauer–Emmet–Teller (BET) surface areas were measured using Tristar II 3020 instrument to measure the adsorption of nitrogen.

Measurement of Electrochemical Performance

The electrochemical properties were evaluated by assembly of 2025 coin cells in a glove box filled with pure argon gas. Lithium pellets were used as the anode, 1 M solution of $LiPF_6$ in ethylene carbon (EC)/dimethyl carbonate (DMC) was used as electrolyte, and the cathode electrodes were obtained with 70% 3D porous V_2O_5 hierarchical microplates active material, 20% acetylene black and 10% poly (tetrafluoroethylene) (PTFE). Galvanostatic charge/discharge cycling was studied in a potential range of 2.4 - 4.0 V vs. Li/Li^+ with a multichannel battery testing system (LAND CT2001A). Cyclic voltammetry (CV) and AC-

impedance spectra were tested with an electrochemical workstation (Autolab PGSTAT 302N).

Results and Discussion

The schematic illustration of the synthesis of 3D porous V_2O_5 hierarchical microplates is shown in Figure 1a. The first step of synthesis involves the dissolution of NH_4VO_3 particles in water bath process. The formation mechanism of NH_4VO_3 quasi-hexagonal microplates may be attributed to the anisotropic growth of their inherent crystal structure and chemical potential in solution,[38,39] which can be confirmed by the FESEM images of the products with different solvothermal reaction time (Figure S1). In this step, the ammonia derived from urea restrains the hydrolysis of ammonium metavanadate effectively (Equation 1-3). As a result, the pure ammonium metavanadate microstructure can be obtained after solvothermal reaction. In addition, urea shows certain ability to dissociate particles and affect the particles' aggregation through direct binding to the particles' surface.[40] Ultimately, the prepared NH_4VO_3 quasi-hexagonal microplates were decomposed into 3D porous V_2O_5 hierarchical microplates under annealing process, corresponding to Equation (4).

$$NH_4VO_3 \leftrightarrow NH_4^+ + VO_3^- \quad (1)$$

$$(NH_2)_2CO + H_2O \rightarrow 2NH_3 + CO_2 \quad (2)$$

$$NH_3 + H_2O \leftrightarrow NH_4^+ + OH^- \quad (3)$$

$$2NH_4VO_3 \rightarrow 2NH_3 + V_2O_5 + H_2O \quad (4)$$

Owing to a conversion from NH_4VO_3 to its corresponding oxides, which makes use of the volume shrinkage and release of internally born ammonia (NH_3) in the process of thermal decomposition, 3D porous V_2O_5 hierarchical microplates were finally obtained. Vanadium oxide layer blocking the gas release effectively is broken by ammonia sealed, forming a small void/pore. Many such processes can concurrently/continuously occur from the outer to inner part of the crystals until continuous channels are eventually formed, while NH_4VO_3 is completely decomposed to V_2O_5. [41,42]

The morphology and microstructure of the as-prepared products were examined by FESEM and TEM. The FESEM and TEM images (Figure 1b, c) reveal that the NH_4VO_3 sample prepared by solvothermal method is composed of the quasi-hexagonal microplates with lengths of more than 10 μm. Energy dispersive spectroscopy (EDS) element mapping analysis (Figure 1d) indicates that V, N and O distribute in NH_4VO_3 quasi-hexagonal microplates. Apparently, Figure 1e, S2 and S3 show that the material morphology is essentially preserved during the annealing and solid-phase conversion process, and the porous structure can be also observed on the surface of V_2O_5 sample calcined at 350 °C (V_2O_5-350). The representative TEM image (Figure 1f) shows the prepared V_2O_5 quasi-hexagonal microplates are composed of interconnected nanosized subunits with highly porous structure. In the HRTEM image (Figure 1g) taken from a edge of a nanosized subunits, the lattice fringes are clearly visible with spacing of 0.34 nm, which is in agreement with that of the (110) planes of V_2O_5 (JCPDS card No. 00-041-1426). There are some irregular particles can be observed in resultant products (Figure S4), their conversion to porous V_2O_5 is similar to that of V_2O_5 quasi-hexagonal microplates (Figure S5).

The resultant products were characterized by XRD to identify the crystallographic structure and crystallinity (Figure 2a). It can be observed that all of the peaks match those of orthorhombic

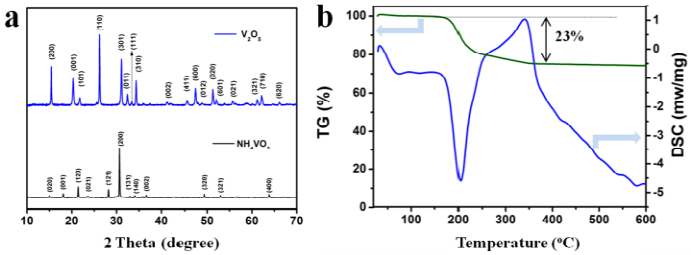

Figure 2. (a) XRD patterns of the prepared products before and after annealing. (b) TG analysis of 3D porous V_2O_5 hierarchical plates in air.

NH_4VO_3 (JCPDS NO. 00-025-0047, space group: *Pmab*, a = 5.8270 Å, b = 11.7820 Å, c = 4.9050 Å) and orthorhombic V_2O_5 (JCPDS NO. 00-041-1426, space group: *Pmmn*, a = 11.5160 Å, b = 3.5656 Å, c = 4.3727 Å). The strong and narrow peaks indicate a high crystallinity of the as-prepared products. In order to confirm the phase transition, Thermogravimetric (TG) analysis of the NH_4VO_3 quasi-hexagonal microplates was carried out in air atmosphere (Figure 2b). The TG curve shows one main step which is related to decomposition of NH_4VO_3 quasi-hexagonal microplates, which can be confirmed by the endothermic peak (~200 °C) of the differential scanning calorimetry (DSC) curve. The weight loss is 23 %, and the value is close to the theoretical weight loss of decomposition of NH_4VO_3 (22.3 %), redundant weight loss may be attributed to the decomposition of residualorganics. The DSC curve also exhibits an exothermic peak at ~350 °C, it is confirmed that there is a phase transformation of V_2O_5.

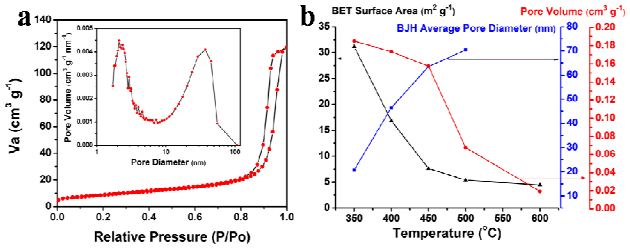

Figure 3. (a) Nitrogen adsorption-desorption isotherms of V_2O_5-350 and corresponding pore size distribution (inset). (b) BET surface area distribution, average pore diameter and pore volume of V_2O_5 samples with different calcination temperatures.

Nitrogen adsorption-desorption isotherms were further measured to characterize the porous structure of the products. It is found that V_2O_5-350 has Brurauer–Emmerr–Teller (BET) surface areas of 32 m^2 g^{-1} with mesopores and macropores from 2–5 to 10–100 nm on the basis of the Barrett-Joyner-Halenda (BJH) methed (inset of Figure 3a). The sorption isotherms of V_2O_5-350 (Figure 3a) appear to be type IV curves, with the H3 hysteresis loops that can be linked to slit-shaped pores. Figure 3b shows that with calcination temperature increasing, average pore diameter of V_2O_5 sample increases, whereas the BET surface area and pore volume of V_2O_5 sample decreases, suggesting porous structure of the products was changed (Figure S6, S7). The BET surface area of V_2O_5 sample annealed at 600 °C decreased to ~5 m^2 g^{-1}, pore structure does not exist according to the low BET

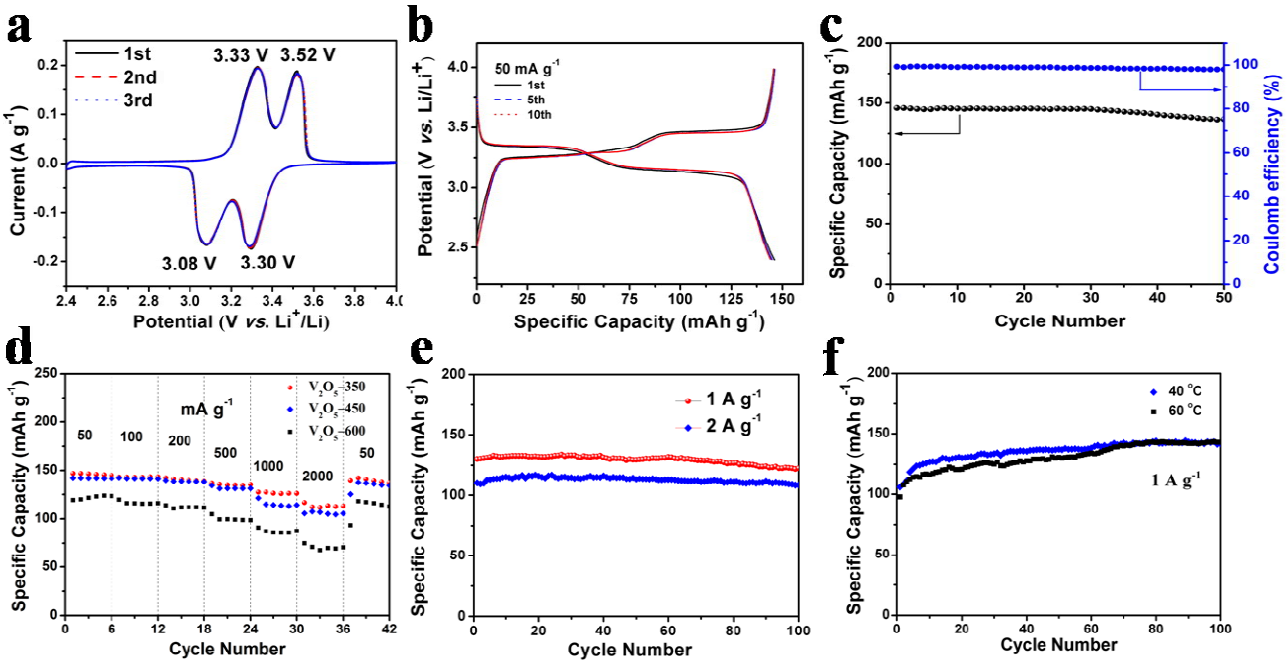

Figure 4. (a) Cyclic voltammograms at a scan rate of 0.1 mV s^{-1} of V_2O_5-350; (b) discharge/charge curves of the first, fifth and tenth cycles at 50 mA g^{-1} of V_2O_5-350; (c) cycling performance at the current density of 100 mA g^{-1} of V_2O_5-350; (d) the rate performance of porous V_2O_5 microplates annealed at different temperatures; (e) cycling performance at high rates of 1 A g^{-1} and 2 A g^{-1} of V_2O_5-350; (f) cycling performance at the current density of 1 A g^{-1} measurement at 40 and 60 °C of V_2O_5-350.

surface area and unavailable pore size data. We also annealed the bulk NH_4VO_3 at 350 °C (Figure S8), whose BET surface area (21 m^2 g^{-1}) and pore volume (0.15 cm^3 g^{-1}) are lower than porous V_2O_5 microplates calcined at the same temperature.

Coin cells with metallic lithium as anode were assembled to investigate the electrochemical performance of the 3D porous V_2O_5 hierarchical microplates cathodes. Cyclic voltammogram (CV) of the porous V_2O_5 microplates was measured at a scan rate of 0.1 mV s^{-1} in the potential range from 2.4 to 4.0 V (Figure 4a). The cathodic and anodic peaks are ascribed to the lithium ion insertion and extraction, respectively. Two main cathodic peaks appear at potentials of 3.30 and 3.08 V, corresponding to the phase transformations from α-V_2O_5 to ε-$Li_{0.5}V_2O_5$ and δ-LiV_2O_5, the processes of which are expressed in Equation 5 and 6, respectively.[40,43]

$$V_2O_5 + 0.5Li^+ + 0.5e^- = \varepsilon\text{-}Li_{0.5}V_2O_5 \quad (5)$$

$$\varepsilon\text{-}Li_{0.5}V_2O_5 + 0.5Li^+ + 0.5e^- = \delta\text{-}LiV_2O_5 \quad (6)$$

In the subsequent scans, the shapes of the curves are almost identical, which indicates good reversibility of the lithium insertion process. Figure 4b displays the discharge/charge curves of the V_2O_5 cathodes at different cycles. The result shows that the discharge/charge curves are almost superposed during 10 cycles. Two voltage plateaus are clearly observed which is quite consistent with the CV curves. The cycling performance was further evaluated by galvanostatic discharge/charge testing. As shown in Figure 4c, the initial discharge capacities of 3D porous V_2O_5 hierarchical microplates is 146 mAh g^{-1} at 100 mA g^{-1}, very close to the theoretical value of 147 mAh g^{-1} for the formation of δ-LiV_2O_5. After 50 cycles, their discharge capacities of 137 mAh g^{-1} are still remained, corresponding to 93.8% of the initial capacity. During the entire cycles, the coulombic efficiency maintains at a high level of more than 99%, demonstrating a good reversibility between the charge and discharge processes.

To evaluate the rate capability, the 3D porous V_2O_5 hierarchical microplates cathode was cycled at various rates, ranging from 50 to 2000 mA g^{-1} (Figure 4d). As the rate increases from 50 to 2000 mA g^{-1}, the discharge capacity of the cathodes decreases gradually from 147 to 112 mAh g^{-1}. After the high rate measurement, when rate is reduced back to 50 mA g^{-1}, a discharge capacity of 139 mAh g^{-1} can be recovered. It is obvious that the rate performance of V_2O_5-350 is better than that of samples annealed at 450 (V_2O_5-450) and 600 °C (V_2O_5-600). Moreover, cycling performance of the 3D porous V_2O_5 hierarchical microplates cathodes at high rates of 1000 mA g^{-1} and 2000 mA g^{-1} are shown in Figure 4e. The initial specific discharge capacities were 130 and 110 mAh g^{-1} at the rates of 1000 and 2000 mA g^{-1}, respectively. Remarkably, their capacities were retained to 123 and 108 mAh g^{-1} after 100 cycles, corresponding to 94.6% and 98.2% of their initial capacity, respectively. In order to investigate the influence of porous structure on the electrochemical performance of V_2O_5, the electrochemical characterizations of the bulk V_2O_5 powders were also measured (Figure S9, S10). The electrochemical performance of the 3D porous V_2O_5 hierarchical microplates is good compared to that of many reported V_2O_5 electrodes, in terms of high-rate capability and cycling performance (Table S1). The electrochemical impedance spectra (EIS) were used to provide further insights (Figure S11). The Nyquist plots indicate that the charge transfer resistance (Rct) of V_2O_5-350 with higher BET surface area is much lower than that of the other two cathodes. The reason for that should be the porous structure with larger surface area results in an more efficient and increases contact area between the active sites and electrolytes, as well as the shorter diffusion distance for Li^+ ions, which leads to rapid ion diffusion and an efficient charge transfer.[44] As a device that delivers high power, the Joule effect must be considered since

large heat can be generated during the charge/discharge process at high power.[45] Therefore, it is crucial to study the temperature-dependent performance. Figure 4f clearly shows that with the increase of cycle number, the capacities at 1000 mA g^{-1} tended to increase both at 40 and 60 °C. The gradual improvement of capacity could suggest the gradual penetration of electrolyte into the particles' interior [46] and the electrochemical kinetics promoted gradually during the temperature-rise process of the cells measured.[47] Significantly, their capacities were 141 and 143 mAh g^{-1} after 100 cycles, respectively, which were higher than the capacities measured at room-temperature. It demonstrates that the porous V_2O_5 hierarchical microplates cathode shows a high rate capacity.

The improved rate capability and cycling stability are attributed to the interesting 3D porous structure. More specifically, the porous structure would facilitate the electrolyte penetration and increase the contact area between the electrode material and the electrolyte.[48] The nanosized V_2O_5 subunits with many spaces between each other have an increased portion of exposed surfaces, which ensure a high utilization of electrode materials and provide more electrochemically active sites for Li^+ to accesses, thus a high capacity is achieved.[49] Moreover, the porous structure might be also an advantage to accommodate the volume variations during the Li^+ ions intercalation and deintercalation.[50] Finally, the nanosized building blocks reduce the distance for Li^+ ions diffusion and the electron transport.[50, 51] In brief, the porous structure is beneficial to the improved cycling stability and excellent rate capability of the 3D porous V_2O_5 hierarchical microplates.

Conclusions

A facile top-down fabrication approach has been developed to prepare 3D porous V_2O_5 hierarchical quasi-hexagonal microplates, via one-step thermal decomposition of NH_4VO_3 microplates. The as-synthesized V_2O_5 microplates are composed of well-defined nanosized subunits, forming a highly porous hierarchical structure which gives rise to high surface area (32 m^2 g^{-1}). When evaluated as a cathode material for lithium batteries, the V_2O_5 microplates display relatively stable capacity retention (capacity retention reach up to 98.2% after 100 cycles). They also show excellent rate capability, with a capacity of 110 mA h g^{-1} at 2000 mA g^{-1}. The excellent electrochemical performance suggests that the unique porous V_2O_5 hierarchical microplates is a promising cathode material for lithium batteries. This one-step thermal conversion of NH_4VO_3 into porous structures can further be applied to converting ammonium salt into such porous structures. Meanwhile, it is convinced that this effective top-down stratagy can be extended to fabricate other micro/nano materials with unique structures which have advanced electrochemical properties.

Acknowledgements

This work was supported by the National Basic Research Program of China (2013CB934103, 2012CB933003), the National Natural Science Foundation of China (51072153, 51272197), the Program for New Century Excellent Talents in University (NCET-10-0661) and the Fundamental Research Funds for the Central Universities (2013-VII-028). Thanks to Prof. C. M. Lieber of Harvard University, Prof. Dongyuan Zhao of Fundan University and Dr. Jun Liu of Pacific Northwest National Laboratory for strong support and stimulating discussions.

Notes and references

[a] *State Key Laboratory of Advanced Technology for Materials Synthesis and Processing, WUT-Harvard Joint Nano Key Laboratory, Wuhan University of Technology, Wuhan 430070, P. R. China. Fax: +86-27-87644867; Tel: +86-27-87467595; E-mail: mlq518@whut.edu.cn*

† Electronic Supplementary Information (ESI) available: SEM images of the samples synthesized under different solvothermal times, EDS mapping of the porous V_2O_5 hierarchical microplate, SEM images of NH_4VO_3 microplates, TEM image of irregular V_2O_5 particle, SEM images of V_2O_5 annealed at different temperatures, nitrogen adsorption-desorption isotherms of porous V_2O_5 microplates and corresponding pore size distribution annealed at different temperatures, SEM images of NV-350, nitrogen adsorption-desorption isotherms of NV-350 and corresponding pore size distribution, SEM images and electrochemical characterizations of the bulk V_2O_5, AC-impedance spectra of V_2O_5 electrodes prepared under different calcination temperatures. See DOI: 10.1039/b000000x/

‡ Author contributions: Qinyou An and Pengfei Zhang contributed equally to this work. All authors discussed the results and commented on the manuscript. The authors declare no competing financial interest.

1 K. T. Nam, D. W. Kim, P. J. Yoo, C. Y. Chiang, N. Meethong, P. T. Hammond, Y. M. Chiang and A. M. Belcher, *Science*, 2006, **312**, 885.
2 B. Kang and G. Cede, *Nature*, 2009, **458**, 190.
3 a) M. Y. Ge, J. P. Rong, X. Fang and C. W. Zhou, *Nano Lett.*, 2012, **12**, 2318. b) N. Mahmood, C. Z. Zhang and Y. L. Hou, *Small*, 2013, **9**, 1321.
4 H. Li, Z. X. Wang, L. Q. Chen and X. J. Huang, *Adv. Mater.*, 2009, **21**, 4593.
5 A. S. Arico, P. G. Bruce, B. Scrosati, J. M. Tarascon and W. V. Schalkwijk, *Nat. Mater.*, 2005, **4**, 366.
6 N. S. Choi, Y. Yao, Y. Cui and J. Cho, *J. Mater. Chem.*, 2011, **21**, 9825.
7 J. M. Tarascon and M. Armand, *Nature*, 2001, **414**, 359.
8 a) M. Armand and J. M. Tarascon, *Nature*, 2008, **451**, 652. b) J. P. Liu, J. Jiang, C. W. Cheng, H. X. Li, J. X. Zhang, H. Gong and H. J. Fan, *Adv. Mater.*, 2011, **23**, 2076.
9 J. B. Goodenough and Y. Kim, *Chem.Mater.*, 2009, **22**, 587.
10 C. K. Chan, H. L. Peng, G. Liu, K. McIlwrath, X. F. Zhang, R. A. Huggins and Y. Cui, *Nat. Nanotechnol.*, 2008, **3**, 31.
11 M. S. Whittingham, *Chem. Rev.*, 2004, **104**, 4271.
12 M. V. Reddy, G. V. Subba Rao and B. V. R. Chowdari, *Chem. Rev.*, 2013, **113**, 5364.
13 S. Q. Wang, S. R. Li, Y. Sun, X. Y. Feng and C. H. Chen, *Energy Environ. Sci.*, 2011, **4**, 2854.
14 Q. T. Qu, Y. S. Zhu, X. W. Gao and Y. P. Wu. *Adv. Energy Mater.*, 2012, ***2***, 950.
15 S. Zhou, X. G. Yang, Y. J. Lin, J. Xie and D. W. Wang, *ACS Nano*, 2012, **6**, 919.
16 Y. Wang and G. Z. Cao, *Adv. Mater.*, 2008, **20**, 2251.
17 T. Y. Zhai, H. M. Liu, H. Q. Li, X. S. Fang, M. Y. Liao, L. Li, H. S. Zhou, Y. Koide, Y. Bando and D. Golberg, *Adv. Mater.*, 2010, **22**, 2547.
18 M. S. Whittinham, *J. Electrochem. Soc.*, 1976, **123**, 315.
19 E. Hosono, T. Kudo, I. Honma, H. Matsuda and H. S. Zhou, *Nano Lett.*, 2009, ***9***, 1045.
20 A. R. Armstrong and P. G. Bruce, *Nature*, 1996, **381**, 499.
21 C. Ban, N. A. Chernova and M. S. Whittingham, *Electrochem. Commun.*, 2009, **11**, 522.
22 J. Muster, G. T. Kim, V. Krstic, J. G. Park, Y. W. Park, S. Roth and M. Burghard, *Adv. Mater.*, 2000, **12**, 420.
23 T. Watanabe, Y. Ikeda, T. Ono, M. Hibino, M. Hosoda, K. Sakai and T. Kudo, *Solid State Ionics*, 2002, **151**, 313.
24 A. M. Cao, J. S. Hu, H. P. Liang and L. J. Wan, *Angew. Chem. Int. Ed.*, 2005**, 44**, 4391.
25 C. F. Zhang, Z. X. Chen, Z. P. Guo and X. W. Lou, *Energy Environ.*

Sci., 2013, **6**, 974.
26 L. Q. Mai, Y. J. Dong, L. Xu and C. H. Han, *Nano Lett.*, 2010, **10**, 4273.
27 T. Y. Zhai, H. M. Liu, H. Q. Li, X. S. Fang, M. Y. Liao, H. S. Zhou, Y. Koide, Y. Bando and D. Golberg, *Adv. Mater.*, 2010, **22**, 2547.
28 a) Y. Wang, K. Takahashi, K. H. Lee and G. Z. Cao, *Adv. Funct. Mater.*, 2006, **16**, 1133. b) S. Q. Wang, Z. D. Lu, D. Wang, C. G. Li, C. H. Chen and Y. D. Yin, *J. Mater. Chem.*, 2011, **21**, 6365. c) C. K. Chan, H. L. Peng, R. D. Twesten, K. Jarausch, X. F. Zhang and Y. Cui, *Nano Lett.*, 2007, **7**, 490.
29 Y. W. Li, J. H. Yao, E. Uchaker, J. W. Yang, Y. X. Huang, M. Zhang and G. Z. Cao, *Adv. Energy Mater.*, 2013, **3**, 1171.
30 A. Q. Pan, H. B. Wu, L. Yu and X. W. Lou, *Angew. Chem. Int. Ed.*, 2013, **125**, 2282.
31 Y. G. Guo, J. S. Hu and L. J. Wan, *Adv. Mater.*, 2008, **20**, 2878.
32 a) H. Liu , D. Su , R. Zhou , B. Sun, G. Wang and S. Z. Qiao, *Adv. Energy Mater.*, 2012, **2**, 970. b) H. Liu, X. Du, X. Xing, G. Wang and S. Z. Qiao, *Chem. Commun.*, 2012, **48**, 865. c) H. Liu, D. Su, G. Wang and S. Z. Qiao, *J. Mater. Chem.*, 2012, **22**, 17437.
33 Y. Q. Qiao, J. P. Tu, X. L. Wang, D. Zhang, J. Y. Xiang, Y. J. Mai and C. D. Gu, *J. Power Sources*, 2011, **196**, 7715.
34 Q. T. Qu, L. J. Fu, X. Y. Zhan, D. Samuelis, J. Maier, L. Li, S. Tian, Z. H. Li and Y. P. Wu, *Energy Environ. Sci.*, 2011, **4**, 3985.
35 a) J. Y. Xiang, X. L. Wang, J. Zhong, D. Zhang and J. P. Tu, *J. Power Sources*, 2011, **196**, 379; b) F. Yu, J. J. Zhang, Y. F. Yang and G. Z. Song, *J. Mater. Chem.*, 2009, **19**, 9121.
36 a) Y. L. Zhao, L. Xu, L. Q. Mai, C. H. Han, Q. Y. An, X. Xu, X. Liu and Q. J. Zhang, *Proc. Natl. Acad. Sci. USA*, 2012, **109**, 19569; b) L. Q. Mai, F. Yang, Y. L. Zhao, X. Xu, L. Xu and Y. Z. Luo, *Nat. Commun.*, 2011, **2**, 381.
37 V. Valtchev and L. Tosheva, *Chem. Rev.*, 2013, **113**, 6734.
38 X. Wang and Y. Li, *Angew. Chem. Int. Ed.* 2002, **41**, 4790.
39 W. Lu, Y. Ding, Y. Chen, Z. L Wang and J. Fang, *J. Am. Chem. Soc.* 2005, **127**, 10112.
40 X. F. Zhang, K. X. Wang, X. Wei and J. S. Chen, *Chem. Mater.*, 2011, **23**, 5290.
41 H. Yu, D. Wang, and M. Y. Han, *J. Am. Chem. Soc.* 2007, **129**, 233.
42 J. Liu and D. Xue, *Adv. Mater.,* 2008, **20**, 2622.
43 Q. Y. An, Q. L. Wei, L. Q. Mai, J. Y. Fei, X. Xu, Y. L. Zhao, M. Y. Yan, P. F. Zhang and S. Z. Huang, *Phys. Chem. Chem. Phys.*, 2013, **15**, 16828.
44 a) B. G. Choi, S. J. Chang, Y. B. Lee, J. S. Bae, H. J. Kim and Y. S. Huh, *Nanoscale*, 2012, **4**, 5924. b) Q. Qu, L. Fu, X. Zhan, D. Samuelis, J. Maier, L. Li, S. Tian, Z. Li and Y. Wu, *Energy Environ. Sci*., 2011, **4**, 3985
45 K. Zaghib, J. B. Goodenough, A. Mauger and C. Julien, *J. Power Sources*, 2009, **194**, 1021.
46 a) R. Dominko, M. Bele, M. Gaberscek, M. Remskar, D. Hanzel, J. M. Goupil, S. Pejovnik and J. Jamnik, *J. Power Sources,* 2006, **153**, 274. b) K. S. Park, S. B. Schougaard and J. B. Goodenough, *Adv. Mater.,* 2007, **19**, 848. c) X. L. Wu, L. Y. Jiang, F. F. Cao, Y. G. Guo and L. J. Wan, *Adv. Mater*., 2009, **21**, 2710. d) R. Dominko, J. M. Goupil, M. Gaberscek, M. Remskar, D. Hanzel and J. Jamnik, *J. Electrochem. Soc.,* 2005, **152**, A858.
47 S. Franger, F. L. Cras, C. Bourbon, H. Rouault, *J. Power Sources,* 2003, **119**, 252.
48 N. Jayaprakash, J. Shen, S. S. Moganty, A. Corona and L. A. Archer, *Angew. Chem. Int. Ed.*, 2011, **50**, 5904.
49 A. Q. Pan, T. Zhu, H. B. Wu and X. W. Lou, *Chem-Eur J.*, 2013, **19**, 494.
50 D. Y. Chen, X. Mei, G. Ji, M. H. Lu, J. P. Xie, J. M. Lu and J. Y. Lee, *Angew. Chem. Int. Ed*., 2012, **51**, 2409.
51 S. Q. Wang, Z. D. Lu, D. Wang, C. G. Li, C. H. Chen and Y. D. Yin, *J. Mater. Chem.*, 2011, **21**, 6365.